Overview of the MicroPrecision Interferometer Testbed

Gregory W. NEAT, Alex ABRAMOVICI, Renaud GOULLIOUD, Robert P. KORECHOFF,
Robert J. CALVET, and Sanjay S. JOSHI
Jet Propulsion Laboratory,
California Institute of Technology
4800 Oak Grove Drive
Pasadena, CA 91109

Abstract

This paper gives an overview the Micro-Precision Interferometer (MPI) testbed and its major achievements to date related to mitigating risk for future spaceborne optical interferometer missions. The MPI testbed is a ground-based hardware model of a future spaceborne interferometer. The three primary objectives of the testbed are to: (1) demonstrate the 10 nm positional stability requirement in the ambient lab disturbance environment, (2) predict whether the 10 nm positional stability requirement can be achieved in the anticipated on-orbit disturbance environment, and (3) validate integrated modeling tools that will ultimately be used to design the actual space missions. This paper presents results which represent the latest advancements made on the testbed in the first two areas. Encouraging results from this testbed confirm that MPI provides an essential link between the extensive ongoing ground-based interferometer technology development activities and the technology needs of future spaceborne optical interferometers. Due to space limitations, all citations can be found in the bibliography of reference [1], which gives an expanded overview of MPI activities.

1. MPI OVERVIEW

Figure 1 shows a bird's eye view of the MPI testbed. Located at JPL, the MPI testbed is a ground-based, suspended hardware model of a future space-based interferometer. Subsystems include: a 7m x 7m x 6.5m softly suspended truss structure with the necessary mounting plates for subsystem hardware; a six-axis vibration isolation system which can support a reaction wheel assembly to provide a flight-like input disturbance source; a complete Michelson interferometer; internal and external metrology systems; and a star simulator that injects the stellar signal into the interferometer collecting apertures.

MPI was built as a testbed for the Science Interferometer Mission (SIM) flight project. In order to operate properly, SIM must maintain positional stabilities of 10 nanometers for specific optical components in the face of several disturbance sources. To achieve the vibration attenuation needed to meet such strict requirements,

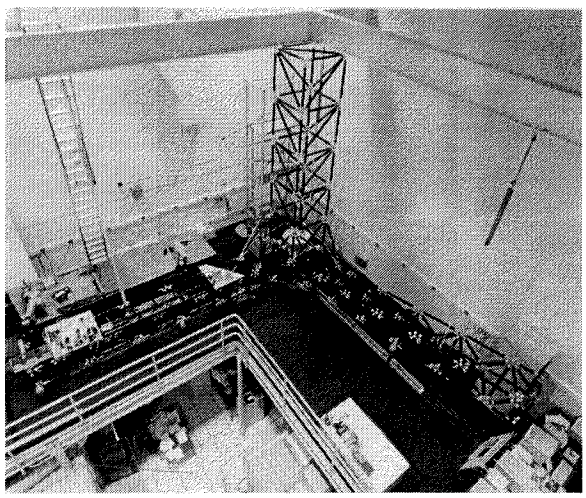

Figure 1: Bird's eye view of the MPI testbed.

the NASA Interferometry Technology Program has formulated a three layered approach shown in Figure 2. The

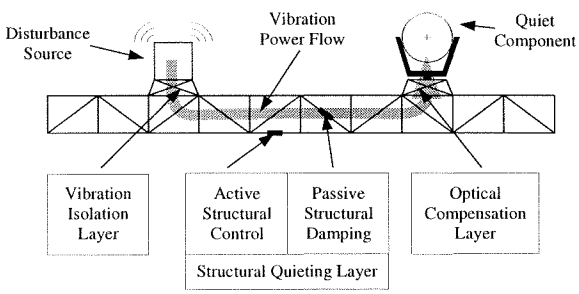

Figure 2: Interferometer Technology Program's layered control approach.

approach is formulated in terms of the three vibration attenuation layers: vibration isolation, structural quieting, and active optics. The strategy is to isolate vibrating machinery at the point of attachment, to damp specific undesirable structural modes that limit optical control system bandwidths, and to actively control specific optical elements to achieve the desired optical performance.

The primary objectives of the MPI testbed related

to vibration attenuation performance are to: (1) demonstrate the 10 nm positional stability requirement in the ambient lab disturbance environment, (2) predict whether the 10 nm positional stability requirement can be achieved in the anticipated on-orbit disturbance environment, and (3) validate integrated modeling tools that will ultimately be used to design the actual space missions. This paper presents results which represent the latest advancements made on the testbed in the first two areas.

The testbed evolution has followed a phased delivery [Neat, Sword, et.al (1993)]. Each phase is marked by a major configuration change by following a design, procurement, integration and test sequence. The first major delivery was the bare structure in 1991 [Sword & Carne (1993)]. The next major delivery was the first interferometer baseline with the six-axis isolation system in 1994 [Neat, O'Brien, et. al. (1995)]. The testbed is presently well into the test phase of the single interferometer configuration. The paper describes this testbed configuration and results from this phase.

2. DISTURBANCE SOURCES

2.1. Ambient Laboratory

This disturbance class includes all sources that affect the interferometer in measurements that will not exist in space. Examples of these sources include building air conditioning, computer cooling fans, gravity, and people walking. These sources manifest themselves as motions of the pseudo star, optical mounts, swaying structure, air turbulence etc. Together these motions from the ambient environment cause RMS motions in optical metrics approximately a factor of 10 higher than what is expected on-orbit. Though the ambient disturbance source is concentrated primarily at low frequency, achieving nanometer positional stabilities in this environment is a challenging problem.

2.2. On-orbit

This class of disturbances includes all sources that are anticipated in the on-orbit environment. The predominant identified source to date are the spacecraft reaction wheel assemblies. Although wheel size is still in question, the SIM design baselines the HST RWA's primarily because these wheels are the quietest wheels flown to date. Fortunately, the HST RWA's have been modeled based on measurements of flight units [Hasha (1986)]. In this model, each wheel produces disturbances in five degrees-of-freedom: one axial force (along the wheel spin axis), two radial forces (normal to the spin axis), and two radial torques (wheel wobble). These disturbances result from wheel imbalances and bearing imperfections and are harmonics of the wheel speed with amplitudes proportional to wheel speed squared [Hasha (1986)].

3. CONTROL APPROACH

This section describes the overall vibration attenuation strategy while the instrument is in observing mode. The strategy differs depending on which disturbance rejection problem is being addressed; the ambient lab disturbance or the on-orbit disturbance. Within the context of the layered control strategy depicted in Figure 2, the differences are in optical loop bandwidths and isolation system contribution to the disturbance rejection performance. For the ambient disturbance rejection problem, no limit is given for closed loop bandwidths. Limitations are thus imposed by actuator, sensor or sample rate limitations for example. For the on-orbit disturbance rejection problem, the sensors dictate the closed loop bandwidth based on known limitations on stellar magnitudes anticipated for this mission. This limitation is set at $300Hz$. The other major difference regards the isolation system. In the ambient disturbance rejection case, this vibration attenuation layer does not participate in improving end-to-end performance since disturbances enter from all directions. This contrasts to the on-orbit case in which the primary disturbance source is the RWA's which interface to the structure through the isolation system.

As a first cut, the MPI testbed adopted a broadband control strategy to meet these requirements. For the isolation system, this means as soft as possible without interfering with the attitude control system and to accommodate limitations imposed by gravity. For the optics, this means maximum disturbance rejection, from dc to $300Hz$. The function of the MPI testbed is to show how well the RWA disturbance can be rejected given these constraints.

4. SYSTEM DESCRIPTION

Figure 3 shows a system level block diagram of the primary elements that compose the MPI testbed and their relationship to each other. This section discusses each of these elements individually.

4.1. Structure

The structure is made up of drawn thin walled 6061-T6 aluminum tubes. To correct for "non-straight" tubes, each tube was "floated" in precision end fittings while adhesive was injected and cured [Sword & Carne (1993)]. The joint design consists of an aluminum node ball interconnecting two or more struts with "b-nut" interface hardware which allowed simple installation and a mechanism to preload the joints. Details on the structure design and assembly procedures are given in reference [Sword & Carne (1993)]. In the initial bare structure configuration, the first flexible mode of the structure was $7.7Hz$ and had an estimated 1 percent modal damping. Initial modal test results showed the bare structure demonstrated extremely linear behavior [Sword & Carne (1993)].

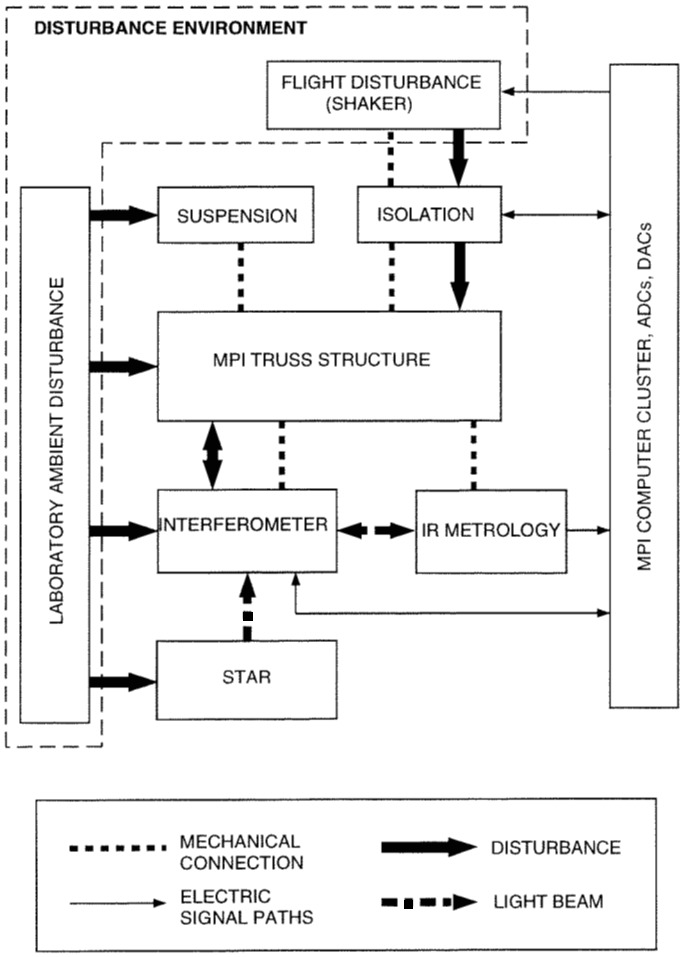

Figure 3: System block diagram showing the relationships between the major MPI testbed subsystems.

4.2. Suspension System/Attitude Control System

An active/passive suspension system supports the testbed from the facility ceiling [Keinholz (1994)]. This system must meet two requirements: (1) isolate the structure from the building, and (2) provide a mechanism to change the rigid body orientation of the structure. The device is made up of two systems. A pneumatic system supports the load of the testbed at the particular support location. This is done by supporting the load by an air cushion. The force is defined by the source air pressure and the area of the device's piston. If the air pressure could be regulated precisely, the pneumatic device would be adequate to support the testbed in a desired vertical position. However, the pressure regulators are not ideal. In parallel with this device is a voice coil actuator which provides a centering function to hold the testbed in the desired position. In addition, the voice coil actuator allows for changes to the testbed's rigid body orientation. Four of these devices (three active, one passive) suspend the testbed from the facility ceiling. With this system, all 6 rigid body modes are in the $0.1Hz$ region.

4.3. Artificial Star

Figure 4 zooms in on the testbed optics boom and traces the stellar optical path through the artificial star and through the testbed optical train. The included schematic diagram calls out important optical components. In addition, the inset in Figure 4 indicates the changes in the stellar beam cross section at the respective locations in the optical path. The following artificial star and interferometer descriptions trace the stellar optical path through the system.

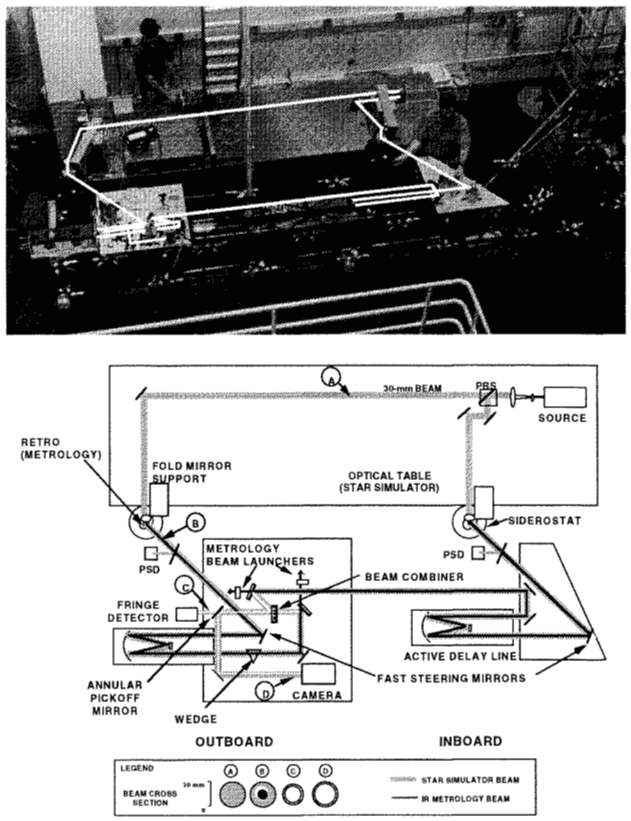

Figure 4: Optical layout for the first MPI baseline from star simulator to optical detectors. The schematic diagram and the photograph depict the same regions of the testbed. The inset shows the beam cross section at different points in the optical path.

The "star" source is the laser head of a commercial laser interferometer system that sits on a pneumatically supported optical table.

4.4. Interferometer

The two interferometer beam paths experience symmetrical reflections in the two interferometer arms on the testbed. The following discussion traces the "inboard" beam path (collecting aperture on the right-hand

side of the figure) without loss of generality. The two-axis gimbaled siderostat mirror contains a 12 mm corner-cube retroreflector used by the internal metrology system. Therefore, the beam leaving the siderostat consists of an annular stellar beam and a central infrared metrology beam. A 90/10 beamsplitter picks off 10% of this beam and sends it to a coarse acquisition sensor (a position sensitive device, PSD), used by the siderostat to initially acquire the star. The remaining light travels to the two-axis, high bandwidth steering mirror which sends the light into the active delay line.

The output beam from the active delay line reflects off three fold mirrors, sending the beam to the "outboard" plate (closest to the collecting aperture on the left-hand side of the figure). The third fold mirror directs the beam from the inboard siderostat to the beam combiner, where it is reflected to join the the transmitted beam from the outboard siderostat. After the beam combiner, the central portion of the combined stellar beams passes through the hole in the annular pick-off mirror to a fringe detector as a single beam with two orthogonally polarized components, with frequencies differing by 1.8 MHz and with a phase difference which depends on the optical path difference for the two arms. The detector, a standard receiver for the commercial interferometer, produces a 1.8 MHz heterodyne signal with a phase that varies as the fringe position of the stellar beams changes. The annular pick-off mirror reflects the outer portion (30 mm OD and 25 mm ID) of each stellar beam towards a digital CCD camera.

Finally, the outboard optical path contains an additional wedge that has a central hole which corresponds to the pick-off mirror hole diameter. This causes the outer annular region of the beam from the outboard siderostat to be deflected by 1 arc minute while the center portion passes undeflected. Thus, at the pick-off mirror, the central portions of the beams are parallel, while the outer regions propagate along directions making a 1 arc minute angle. The two reflected beams are therefore focused at different points on the CCD camera, which allows to sense the pointing of the two beams with a single sensor. The digital image is processed in real time in order to find the centroid of the beam images. The algorithm currently in use determines the position of the image centroid with a resolution of 0.01 pixels. For additional details on the optical system, see [Hines (1995)].

4.5. Metrology System

In addition to the stellar beams, two independent internal metrology beams trace the internal paths (from beam combiner to corner-cube retroreflectors at the siderostats) of each interferometer arm. The external metrology monitors changes in the relative positions of the different interferometer baselines. It does this by launching a large number of metrology beams from the external metrology boom, to each siderostat which contain corner cube retroreflectors in the center. Together, these beams form an optical truss.

4.6. Isolation System

MPI incorporates a six-axis vibration isolation system consisting of a plate attached to the top of a hexapod mount. The top plate provides an interface for actual reaction wheels, rotational shakers or linear translating shakers. The shakers either emulate the reaction wheel disturbance or provide a broadband disturbance input for transfer function measurements. The objective of the isolator is to pass low frequency reaction wheel control torques across the mount while simultaneously preventing the undesirable, high frequency reaction wheel disturbance harmonics from passing across the mount.

The mount design utilizes a passive and active isolation capability. The approach is to enhance the mounts' inherent passive performance with an active stage. The mount consists of 6 identical isolator struts arranged in a mutually orthogonal hexapod configuration. Each strut contains a simple voice coil actuator, a parallel motion flexure that connects the voice coil magnet to the coil (providing the passive stiffness), and a force transducer for feedback. The control strategy is to close six independent SISO loops to actively soften each strut's passive stiffness by a factor of 10-100 thereby moving the mount's passive corner frequencies down by a factor of 3-10. The present system has a 10 Hz passive mount corner frequency. For more details on the isolation system, see reference [Spanos, Rahman, et. al. (1995)].

4.7. Real-Time Computer System

All instrument control functions are provided by a digital real-time computer system. The instrument operator sits at a SUN workstation which is the host to a VME-based system that provides the real-time control functions. These functions range from instrument sequencing through different operating modes to the individual digital controller implementations.

5. MODES OF OPERATION

The primary operating mode of interest on the testbed is when the interferometer "observes" a star. This is the operating mode when the $10nm$ requirement must be demonstrated. However, to reach this condition, as with the on-orbit instrument, requires a large number of initialization, calibration and acquisition procedures. Figure 5 provides a high level sequence of operations that must be executed to reach "observing" mode. All of these sequential operating modes use a subset of the elements described in the System Description section of this paper.

5.1. Coarse Acquisition System

This system is responsible for placing the two incoming stellar beams on the fine pointing camera located at

Figure 5: High-level sequence of operating modes to reach instrument "observing" mode.

the end of the optical train. Quasi-static disturbances such as thermal variations in the lab or dynamic rigid body motions of the star relative to the swaying testbed cause the wave fronts of the two incoming beams to become non-parallel. The coarse acquisition system rejects these low frequency large amplitude (milliradian) disturbances. The pointing error is sensed with a two-dimensional PSD placed in the focal plane of a lens that focuses the beam which is picked off the main beam by a 90/10% beamsplitter. The PSD null position is co-boresighted with the center of the camera located at the end of the optical train. The PSD output is digitized at $2kHz$ and filtered with a second order low pass with a cross-over frequency of $2Hz$. The loops are all decoupled so that the same filter is used for both axes, on both siderostats. The compensator output is fed to the siderostat controller, which generates the signals that operate the micro-stepper motors controlling the two pointing degrees of freedom of the siderostat.

5.2. Fine Pointing System

Once the spots from the two interferometer arms are on the camera, the fine pointing system maintains parallel wavefronts in the presence of the higher frequency disturbances. The fast steering mirror has a bandwidth of 1 kHz and an angular range of 70 arcsecs. Three symmetrically oriented piezo actuators position the mirror, providing tip and tilt motion. The sensor for the pointing control subsystem is a high-frame-rate 32 x 32 pixel CCD camera. During closed loop operation, only a 5 x 5 pixel window is transferred from the camera to the processor enabling high sample rates. The dedicated processor for this loop calculates x, y centroid values for this 5 x 5 image at 4 kHz.

The fundamental approach to the pointing control design is to decouple the x and y tilts resulting in 2 independent single-input, single-output compensators for each interferometer arm. By design, all four of these loops have the same plant transfer function and, therefore, utilize the identical compensator design. The compensator (for all four loops) is 7th order, and provides 60 dB of feedback at low frequency (1 Hz) and the unity gain frequency is $80Hz$. In the presence of the lab ambient noise environment, this control approach stabilizes pointing to 0.27 μrad (RMS) which is a factor of 10 better than the requirement. With the two interferometer arms locked onto the same star, the stellar fringe can now be acquired. See references [Neat, O'Brien, et. al. (1995)][O'Brien & Neat (1995)] for more details on the pointing control subsystem.

5.3. Fringe Acquisition

The present HeNe single frequency stellar source does not require acquisition since the fringe position is not unique. The instrument simply selects the fringe position at start-up time as the central fringe position. Once a white light system is installed, this subsystem will be implemented and tested in the ambient and on-orbit vibration environments.

5.4. Fringe Tracking

The purpose of the fringe tracking subsystem is to equalize stellar pathlength from the target star through each arm of the interferometer to the point they are combined.

The actuator for this subsystem is the active delay line which actually consists of three nested actuators. This three-tiered actuator acts as a linearly translating retroreflector with tremendous dynamic range. A stepper motor provides low frequency (dc), long travel capability (m). An intermediate voice coil actuator translates (cm) the entire cat's-eye assembly in the mid-frequency range (dc - 100 Hz). A reactuated piezo supporting the secondary mirror provides the high bandwidth (kHz) precise actuation stage (μm). The coarse stepper motor is used primarily to slew and acquire a new stellar fringe. Once acquired, this stage is locked down and the other two stages provide the actuation necessary to reject disturbances during an observation.

The MPI fringe detector provides fringe position measurements at 8 kHz. These measurements are subtracted from the desired fringe position (0) to create the error signal to be filtered by the fringe tracker compensator. The bandwidth of the fringe tracking loop is 300 Hz.

The parallel connection of the piezo and voice coil actuators enables rejection of the large amplitude, low frequency disturbances with the large stroke voice coil actuator and the small amplitude , high- frequency disturbances with the piezo actuator. See references [Neat, O'Brien, et. al. (1995)] and [Neat & O'Brien (1996)] for more details on the fringe tracker control system.

6. RESULTS

6.1. Ambient Performance Measurement

Figure 6 shows a step response of the fringe tracker system in the ambient MPI lab disturbance environment. The predominant recognizable disturbance when the loop is open is the one Hz flexure mode of the active delay line. This is likely due to motion of the entire structure which in turn excites the delay line flexure mode. Air turbulence and fluctuations in the air pressure which in turn perturbs the suspension system set point are the sources of these disturbances. Over all frequencies, the fringe position is 1930 nm RMS during this run while the loop is open. With the loop closed, the fringe position jitter is reduced to 8.1 nm RMS. The majority of the energy in this closed loop

fringe position is around 100 Hz and is from the computer cooling fans.

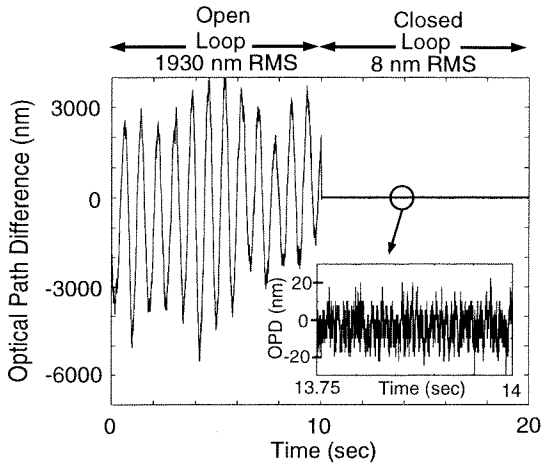

Figure 6: Optical path difference as a function of time for the fringe tracker loop open and closed.

6.2. On-Orbit Performance Prediction

This section presents results showing how the present MPI control design would perform in the on-orbit disturbance environment. The approach to measure on-orbit performance in a ground-based lab setting uses disturbance transfer functions acquired from the MPI testbed combined with an analytical disturbance model of the RWA's. This novel performance prediction algorithm predicts instrument performance in an accurate, efficient way, covering the entire range of possible RWA disturbance conditions that would occur during an instrument observation [Neat & Melody (1996)]. The effectiveness of the layered control technology can be evaluated by predicting instrument performance in three configurations. These configurations are: the no control condition (hard mounted disturbance, no active optics); active optics (hard mounted disturbance, optical control loops operational); and the completely active condition (active isolation of disturbance, optical control loops operational). The six transfer functions (3 forces, 3 torques) from the shaker input mounting location to fringe position output, were measured for each of these configurations.

An example of the parameterized result from this performance prediction algorithm is given in Figure 7. This figure displays the fringe position variation as a function of wheel speed for a single wheel for the three control configurations. There is a separate plot for each of the four reaction wheels.

Norms defined to summarize these parameterized fringe position variation functions into a single number are defined in reference [Neat & Melody (1996)]. For the completely active condition, considering all four wheels, the predicted RMS fringe position is 10.1 nm.

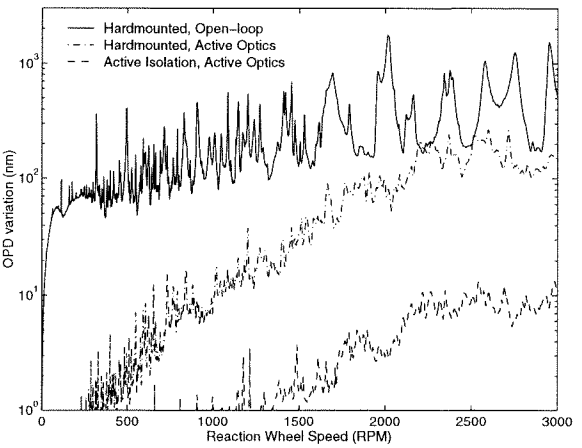

Figure 7: Predicted on-orbit fringe position variation as a function wheel speed for a single wheel.

7. CONCLUSIONS

This paper presented an overview of MPI activities that address vibration attenuation issues for spaceborne optical interferometers. Results from the MPI testbed are very encouraging. For a single interferometer looking at a bright star, the astrometric requirement of 10 nm has been met in both ambient and on-orbit disturbance environment tests. In the future, multiple interferometric baselines will be evaluated.

Additional MPI activities, not presented in this paper, are integrated structural/optical modeling for interferometers [Melody & Neat (1997)]. These activities include validation of the methodology for various closed-loop configurations [Melody & Neat (1997)] and assessing the sensitivity of these results to the accuracy of the structural model [Joshi, Melody, et. al. (1997)].

Acknowledgements

We would like to acknowledge all the past and present members of the MPI team that contributed to this work.

This work was performed at the Jet Propulsion Laboratory, California Institute of Technology, under contract with the National Aeronautics and Space Administration.

References

[1] G. Neat, A. Abramovici, S. Joshi, J.W. Melody, R. Calveat, N. Nerheim, and J. O'Brien,"Control Technology Readiness for Spaceborne Optical Interferometer Missions ," The Space Microdynamics and Accurate Control Symposium, Toulouse, France, May, 1997.